Comparative study of band-structure calculations for type-II InAs/$In_xGa_{1-x}Sb$ strained-layer superlattices

D. N. Talwar* and John P. Loehr
Wright Laboratory, Solid State Electronics Directorate (WL/ELRA), Wright-Patterson Air Force Base, Ohio 45433-6543

B. Jogai
University Research Center, Wright State University, Dayton, Ohio 45435
(Received 7 October 1993; revised manuscript received 21 December 1993)

Short-period InAs/$In_xGa_{1-x}Sb$ superlattices may allow strong optical transitions in the long-wavelength infrared (>10 μm) spectral region. Absorption calculations can be difficult, however, because of the strongly type-II interface and because of the large lattice mismatch. We present a comparative study of band-structure calculations for strained-layer type-II InAs/$In_xGa_{1-x}Sb$ superlattices grown on GaSb. The energy of superlattice band gaps (E_{gs}) and the cutoff wavelengths (λ_c) are computed in the empirical tight-binding, effective-bond-orbital, and 8×8 $\mathbf{k}\cdot\mathbf{p}$ models. In the empirical tight-binding model (ETBM) the strain is included by scaling the matrix elements according to Harrison's universal $1/d^2$ rule and by appropriately modifying the angular dependence. The bond-orbital model (EBOM) and $\mathbf{k}\cdot\mathbf{p}$ calculations include the strain via the deformation-potential theory. We find in all cases that the superlattice band gap decreases rapidly with increasing x and that the proper inclusion of strain is critical in the ETBM. Our results compare favorably with existing experiments. In addition, we compare directly the results of the EBOM and $\mathbf{k}\cdot\mathbf{p}$ models. Contrary to expectations, the two models give quite different results for InAs/InSb superlattices.

I. INTRODUCTION

A significant amount of effort has been devoted in recent years to develop two-dimensional arrays of photovoltaic semiconductor detectors for infrared (ir) imaging in the 10–12-μm wavelength region and beyond.[1–9] Such detectors are usually fabricated from the II-VI mercury cadmium telluride (MCT) $Hg_{1-x}Cd_xTe$ ternary alloy,[10] as no bulk III-V materials have sufficiently small band gaps at 77 K for operation in this wavelength range. There are, however, difficulties associated with fabricating high-performance MCT arrays, especially for wavelengths exceeding 10 μm. The primary problems are: (i) compositional inaccuracies cause variations in the band gap (or equivalently the cutoff wavelength λ_c), (ii) large tunneling dark currents caused by the narrow band gap (<0.1 eV) and the small effective mass result in low specific detectivities, and (iii) high Auger recombination rates further increase the dark current. In view of these difficulties, a large number of III-V semiconductor materials have been proposed[1–9] as alternatives to the conventional MCT alloys for long-wavelength infrared detection applications. These material systems are artificially structured small-band-gap type-II superlattices (SL's) that can be synthesized with advanced epitaxial growth techniques such as molecular-beam epitaxy. If brought to maturity, detectors based upon such SL's are expected to achieved background-limited performance at higher operating temperatures than the MCT-based systems, and can be readily manufactured because of their compatibility with advanced III-V device processing technology. Consequently, numerous SL's (e.g., $InAs_xSb_{1-x}$/$InAs_ySb_{1-y}$,[11–14] InAs/$In_xGa_{1-x}Sb$,[1–9] etc.) with different band-edge lineups strain conditions, and growth orientations have been grown and studied in recent years.

Among others, the type-II InAs/$In_xGa_{1-x}Sb$ strained-layer SL system proposed by Mailhiot and Smith[1] is suggested to have electronic and optical properties superior to those of MCT alloys for cutoff wavelengths λ_c exceeding 10 μm. The conceptual basis for achieving far-infrared energy gaps in the InAs/$In_xGa_{1-x}Sb$ SL system has been discussed at length in the literature.[1] Briefly, a long-wavelength response is predicted based on the misaligned, or type-II, band-edge relationship between the two constituent materials at the interface. The SL system InAs/GaSb falls into the misaligned category because the lower-energy InAs conduction-band edge lies below the valence-band edge of GaSb.[15] Because of this type-II energy-band lineup, the SL can have a band gap smaller than that of either of the constituent materials. Hence, by altering the InAs and GaSb layer thicknesses, the SL band gap (E_{gs}) can be tailored from 0 to 0.8 eV. Semimetallic behavior can be demonstrated in InAs/GaSb but only for comparatively thick layers.[15] Since the electrons tend to be localized in the InAs layers and the holes in the GaSb layers, the electron-hole wave-function overlap and the resulting optical transition matrix elements decrease substantially with increasing SL period. Consequently, for a thick-layer InAs/GaSb SL with band gap less than 0.1 eV, which is required to detect long-wavelength (>10 μm) radiation, the optical absorption coefficient is too small to be practical. It should be mentioned that for type-II SL detection applications, *small* band gaps and *large* optical

0163-1829/94/49(15)/10345(9)/$06.00

matrix elements tend to be mutually exclusive requirements. Inducing strain into the SL, by incorporating In into the GaSb layers, increases the energy separation between the $In_xGa_{1-x}Sb$ heavy-hole valence band and the InAs conduction band. This allows small band gaps to be achieved with sufficiently short periods to provide acceptable absorption coefficients. Following this proposal, a large number of groups[1-9] have reported photoluminescence, photoconductivity, magnetotransport, and optical transmission measurements to estimate the band gaps (E_{gs}) of InAs/$In_xGa_{1-x}Sb$ SL's grown on GaSb substrates.

In this paper we present model calculations for the band gaps E_{gs} and cutoff wavelengths (λ_c) of strained InAs/$In_xGa_{1-x}Sb$ SL's grown on GaSb substrates. In the presence of strain, the SL band-structure calculations become more complicated than those for lattice-matched systems. Previously, $\mathbf{k}\cdot\mathbf{p}$ (Ref. 1) and simple tight-binding calculations[6,7] have been performed to study the band-gap variations in InAs/$In_xGa_{1-x}Sb$ SL's. By using an empirical tight-binding method (ETBM) with an sp^3s^* basis, Shen, Ren, and Dow[4] have recently studied the effects of layer thicknesses on the SL band gap in InAs/GaSb. Assuming a perfectly lattice-matched structure, the authors of Ref. 4 have predicted a semimetallic behavior in $(InAs)_{N_a}/(GaSb)_{10}$ SL's for $N_a > 26$. One of the purposes of this work is to extend the ETBM formalism (see Sec. II A) to strained-layer SL's. By properly incorporating the strain effects, without introducing additional parameters, we compute the effects of layer thickness and In mole fraction x on the fundamental band gap of InAs/$In_xGa_{1-x}Sb$ SL's. Along with the modified ETBM we also consider an eight-band $\mathbf{k}\cdot\mathbf{p}$ and an effective-bond-orbital model (EBOM) (cf. Secs. II B and II C) to study the electronic band structure of InAs/$In_xGa_{1-x}Sb$ SL's. These latter models have the advantage that they can easily incorporate effective-mass information, while the ETBM is expected to have greater validity for very thin layers. In all models, we find that the presence of coherent strain between InAs and $In_xGa_{1-x}Sb$ layers shifts the band edges and further reduces the SL band gap. By increasing the indium composition x, narrower band gaps and cutoff wavelengths in excess of 10 μm can be obtained for thinner SL's (see Sec. III), leading to enhanced optical absorption and carrier transport properties. In Sec. III, we compare these theoretical results with existing magnetooptical and photoconductivity data,[6] and finally we conclude in Sec. IV.

II. THEORETICAL METHODS

Here we describe the band-structure calculations for type-II strained-layer SL's via three different methods: (a) a modified sp^3s^* ETBM, (b) an eight-band $\mathbf{k}\cdot\mathbf{p}$ model, and (c) an effective-bond-orbital model, and discuss their relative strengths and weaknesses. In all calculations, we assume that the SL structure is grown on a GaSb substrate to allow comparison of the calculated E_{gs} with existing experimental data. We assume a rigid substrate, and so the strain in each layer is given by the lattice mismatch between GaSb and the unstrained constituent material. The strain effects are incorporated into the tight-binding framework in a straightforward manner without introducing any additional parameters (see the Appendix), while the $\mathbf{k}\cdot\mathbf{p}$ and EBOM models include strain via the deformation-potential theory.

A. Empirical tight-binding method

The sp^3s^* model to describe the [001] InAs/$In_xGa_{1-x}Sb$ superlattice is a modified version of the one considered recently by Shen, Ren, and Dow.[4] In the sp^3s^* tight-binding formalism, the excited s-like state s^* is added to the conventional sp^3 basis in order to simulate states at higher energy. This method was first proposed by Vögl, Hjalmarson, and Dow[16] to consider only nearest-neighbor interactions and has been extended by Newman and Dow[17] to include some second-nearest-neighbor interactions. The tight-binding parameters have been corrected recently by Yamaguchi.[18] We have used the corrected parameters and have included the second-nearest-neighbor matrix elements (E_{sx}^{0a}, E_{sx}^{0c}, E_{xy}^{0a}, and E_{xy}^{0c}) to ensure better agreement between the calculated and reference energy values (L_{1c} and L_{5v}) of the bulk materials at the L critical point in the Brillouin zone. The superlattice structure considered here consists of N_a two-atom-thick layers of InAs [material $A(c,a)$] and N_b two-atom-thick layers of $In_xGa_{1-x}Sb$ [material $B(c',a')$] repeated periodically, with N_L being the sum of (N_a+N_b). The terms c (c') and a (a') are regarded as the cation and anion atoms of the A (B) material. We denote this superlattice as $(InAs)_{N_a}/(In_xGa_{1-x}Sb)_{N_b}$.

In the standard sp^3s^* formalism, we first construct the following Bloch sums defined by the linear combination of atomic orbitals:

$$\chi_b^{\alpha}(\mathbf{r},\mathbf{k})=\frac{1}{\sqrt{N}}\sum_j \exp[i\mathbf{k}\cdot(\mathbf{r}_b+\mathbf{R}_j)]\phi_b^{\alpha}(\mathbf{r}-\mathbf{R}_j-\mathbf{r}_b)\ . \quad (1)$$

Here α is a quantum number that runs over the basis orbitals s, p_x, p_y, p_z, and s^* on the two types of sites b (either c or a representing the cation and anion, respectively) in the zinc-blende structure; N denotes the number of wave vectors $\mathbf{k}$ in the first Brillouin zone with the origin of the jth unit cell at $\mathbf{R}_j$; and $\mathbf{r}_b$ represents the positions of the neighboring atoms. The SL electronic wave function can be expanded as a linear combination of the Bloch sums:

$$\Psi_{n\mathbf{k}}^{\mathrm{SL}}(\mathbf{r})=\sum_{\alpha b} A_{\alpha b}^{n}\chi_b^{\alpha}(\mathbf{r},\mathbf{k})\ . \quad (2)$$

Since the atomic orbitals are assumed to be orthogonal, the Schrödinger equation in this basis can be written as

$$\sum_{\beta j}[H_{ij}^{\alpha\beta}-E_n(\mathbf{k})\delta_{\alpha\beta}\delta_{ij}]=0\ . \quad (3)$$

Here the terms $H_{ij}^{\alpha\beta}$ represent the interaction integrals between the α orbital of the atom i and the β orbital of the atom j. The solution of these simultaneous equations is obtained by diagonalizing the $10(N_a+N_b)\times 10(N_a+N_b)$ Hamiltonian matrix (see the Appendix for details). In the semiempirical tight-binding framework, the $H_{ij}^{\alpha\beta}$

are generally treated as free parameters and their values are determined by fitting to experimental data such as the band gap and the effective masses. Here, we have obtained strain-free nearest-neighbor tight-binding parameters (see Table I) by fitting almost exactly to the existing nonlocal-pseudopotential band energies of the bulk materials (InAs, InSb, GaAs, and GaSb) at high symmetry points (Γ and X). In order to reproduce the reference band structure at the L critical point, we have also added the second-nearest-neighbor interaction integrals in the tight-binding Hamiltonian. In our study we have considered four sets of parameters (i.e., those of InAs, $In_xGa_{1-x}Sb$, InSb, and $In_xGa_{1-x}As$) to describe appropriately the actual bonding of the atoms in the SL. At the interface, for instance, if the cation is In_xGa_{1-x} and the anion is As(Sb), then the matrix elements of the material $In_xGa_{1-x}As(Sb)$ are obtained in the virtual-crystal approximation by averaging the matrix elements of InAs(Sb) and GaAs(Sb). The second-nearest-neighbor interactions $U_{cc'}$ ($U_{aa'}$) between two cations c and c' (two anions a and a') lying in A and B compound semiconductors can be determined, in principle, by fitting the calculated band to the reference band of the superlattice. However, for the sake of simplicity we use only the average values of the two bulk parameters.

The strain effects are modeled by scaling the "strain-free" tight-binding matrix elements (see Table I) according to Harrison's universal scaling $1/d^2$ rule,[19] where d is the atomic spacing. The effects of bond-angle changes are also treated properly by assuming that the s and p orbitals transform as the appropriate spherical harmonics and that only the two-center interactions are important. This method is quite simple, but is sufficient to investigate the qualitative effects of heterointerface bond relaxation on the electronic structure. Moreover, the advantage of this scheme is that it avoids the introduction of new parameters and/or experimental data to model the strain effects and can be easily applied to other strained systems. Although a similar approach has been incorporated recently by Wu, Fujita, and Fujita,[20] we have clarified some discrepancies in their distance scaling factors and have algebraically simplified the angular factors; we present the results in the Appendix. Once the strained matrix elements are obtained, the intramaterial and intermaterial blocks in the SL Hamiltonian can be formed from them (see the Appendix).

TABLE I. Strain-free tight-binding parameters for the bulk materials (in eV) in the notations of Vögl, Hjalmarson, and Dow (Ref. 16). Four second-nearest neighbor parameters (E_{sx}^{0a}, E_{sx}^{0c}, E_{xy}^{0a}, and E_{xy}^{0c}) are added here to fit the reference band structure at the L critical point.

Parameters	InAs	GaSb	InSb	GaAs
E_{ss}^{a}	−8.36	−6.09	−5.80	−8.36
E_{pp}^{a}	−1.54	−2.67	−1.25	−2.67
E_{ss}^{c}	1.04	1.61	1.90	1.04
E_{pp}^{c}	3.85	3.67	4.14	3.67
$E_{ss^{**}}^{a}$	8.56	8.74	9.03	8.56
$E_{ss^{**}}^{c}$	9.53	9.32	9.82	9.32
V_{ss}^{0}	−4.16	−5.43	−3.61	−6.43
V_{xx}^{0}	2.00	1.86	2.25	1.95
V_{xy}^{0}	3.97	4.38	4.62	5.08
V_{s0p}^{0}	2.62	5.27	5.54	4.25
V_{s1p}^{0}	4.50	4.53	4.81	5.13
$V_{s^*0p}^{0}$	3.76	6.36	6.25	4.75
$V_{s^*1p}^{0}$	4.59	5.77	6.71	5.19
E_{sx}^{0a}	−0.011	0.06	0.231	−0.32
E_{sx}^{0c}	−0.011	0.06	0.231	−0.32
E_{xy}^{0a}	0.003	−0.15	−0.14	−0.21
E_{xy}^{0c}	0.003	−0.15	−0.14	−0.21

As for the valence-band discontinuity of the $InAs/In_xGa_{1-x}Sb$ interface, a conclusive value of ΔE_v has not been established experimentally. In keeping with current practice, though, we assume that the unstrained valence-band edge in the $In_xGa_{1-x}Sb$ layer is always 0.51 eV above the unstrained valence-band edge in the InAs layer for all x.[1] Since the valence-band offset merely fixes the origin in the tight-binding framework, its value is added to the diagonal elements of the Hamiltonian matrix. This operation simply shifts the bulk band structure of the material up or down as a whole and has no effect on its curvature.

B. Eight-band k·p model

For the $\mathbf{k}\cdot\mathbf{p}$ model, we work with the 8×8 Hamiltonian as presented by Kane.[21] The eight basis states consist of the s and p_x, p_y, p_z, states coupled appropriately to the electron spins to give total angular momentum states. We include $\mathbf{k}$-dependent strain effects by following the prescription of Bahder,[22] whereby the Hamiltonian is expanded to first order in the strain tensor as suggested by Pikus and Bir.[23] This represents an improvement over the standard Pollak and Cardona[24] treatment, in which the strain serves only to introduce $\mathbf{k}$-independent constant terms into the Hamiltonian. We take Bahder's deformation potentials, a' and b' to be zero for all materials. For the details and notation of the Hamiltonian itself, we refer the reader to Refs. 22. We calculate the Luttinger parameters and the momentum matrix element for each layer from the bulk band gap and the electron, light-hole heavy-hole, and split-off masses for that layer. The parameter values are presented in Table II. A simple linear average is employed for the ternary compound.

We solve for the superlattice band structure in the effective-mass approximation. Here the bulk 8×8 $\mathbf{k}\cdot\mathbf{p}$ matrix is converted into a set of eight coupled differential equations by replacing k_z with $-id/dz$. These differential equations are then discretized into finite-difference form and the resulting matrix is diagonalized to obtain the superlattice energies and wave functions.[25] The only concern is to symmetrize properly any products of spatially dependent material parameters with k_z *before* converting the equations to differential form. This approach ensures that the probability current is conserved across the heterointerface and that the resulting set of differential equations is Hermitian. For a more detailed description of the symmetrization process, and a rough justification, see Ref. 26.

TABLE II. Material parameters used in the EBOM and $\mathbf{k}\cdot\mathbf{p}$ models. The EBOM matrix elements are determined from Table II, Ref. 27, which should read that $E_{zz}=E_{xx}-X_{hl}/8$ and that $E_{ss}=-(m_0/m_c)R_0+16E_{sx}^2[2/E_g+1/(E_g+\Delta)]/3$. Note also that the $\mathbf{k}\cdot\mathbf{p}$ model uses m_{s0} to set the conduction-valence band coupling, while the EBOM uses $X_{h1}=4$ eV.

Quantity	InAs	GaSb	InSb
m_c	0.023	0.042	0.0133
γ_1	19.74	11.89	34.8
γ_2	8.65	4.92	15.9
γ_3	9.34	5.19	16.29
m_{s0}	0.08	0.13	0.08
Δ (eV)	0.381	0.77	0.81
E_g (eV)	0.426	0.81	0.237
a_0 (Å)	6.0584	6.0959	6.4794
c_{11} (10^{11} dyne/cm^2)	8.33	8.85	6.67
c_{12} (10^{11} dyne/cm^2)	4.53	4.04	3.65
a (eV)	−5.8	−8.28	−7.9
b (eV)	−1.7	−1.8	−1.8

C. Effective-bond-orbital model

The EBOM put forth by Chang[27] is essentially a nearest-neighbor fcc tight-binding model. The primary advantage of this scheme is that the basis set used in the formalism is exactly the same as that used in the 8×8 $\mathbf{k}\cdot\mathbf{p}$ model. Hence, the $\mathbf{k}\cdot\mathbf{p}$ parameters (see Table II) can be directly incorporated into the calculations. We treat the strain with the Pollak and Cardona deformation-potential theory[24] by introducing the appropriate constant terms into the diagonal elements of our bulk tight-binding matrices. We solve for the superlattice band structure by applying the slab method[28] to the fcc tight-binding Hamiltonian: for a more detailed description of this method we refer the reader to Refs. 28. The interface parameters are computed by simple averaging, and we have taken the bulk Hamiltonian directly from Ref. 27, subject to the corrections presented in Table II.

III. RESULTS AND DISCUSSION

An important boundary condition that has been considered in all three model calculations is the band lineup at the interface, as the calculated results are very sensitive to the band alignment. Before strain, it is assumed that the twofold-degenerate valence-band edge in the $In_xGa_{1-x}Sb$ layer is 0.51 eV above the twofold-degenerate valence-band edge in the InAs layer, regardless of x. The uniaxial component of the strain then splits the twofold degeneracy in each layer. The orginal point of reference or "origin" of the valence-band edge in InAs remains fixed relative to that in the $In_xGa_{1-x}Sb$ layer. In the absence of strain-induced light-hole–split-off coupling, these reference points would be in the middle of the split valence-band edge. Because of the strain-induced coupling, though, the midpoints of the split valence bands will lie slightly above their origins. All three models include strain-induced light-hole–split-off coupling. Accordingly, the center of the split valence-band edge in InAs will not be at 0.51 eV below the center of the split valence-band edge in $In_xGa_{1-x}Sb$. This separation will vary with x, but is expected to be within a few percent of 0.51 eV. In all three models, all of the hydrostatic energy shift is assigned to the conduction-band edge. This alignment scheme is similar to that employed in Ref. 1. It is also assumed that the superlattice is grown along the (001) direction on a GaSb substrate. This means that the InAs layers are under an in-plane tensile strain, while the $In_xGa_{1-x}Sb$ layers are under an in-plane compressive strain. Adding indium composition x to the second layer raises the heavy-hole band edge in the $In_xGa_{1-x}Sb$ layer further above the conduction-band edge in InAs, causing the effective band gap to decrease.

Calculations of the SL energy gaps were performed using the above theoretical models for N_a layers of InAs alternating with N_b layers of $In_xGa_{1-x}Sb$. The results for superlattice band gaps E_{gs} and cutoff wavelength λ_c are displayed in Figs. 1(a)–1(c) for the special case of $N_a=N_b$, and for the alloy composition x in the range $0\le x\le0.4$. In Table III, we have compared the calculated values of E_{gs} with the existing experimental data[6] for the three specific SL structures. In each model, the calculated variations of energy gaps show identical trends and are in general agreement, though sample 890 shows the opposite trends from our calculation. This may result from uncertainties in the layer thicknesses and/or compositions. A perusual of Figs. 1(a)–1(c) reveals two important facts about the significance of type-II SL's for long-wavelength ir detection applications. These facts are: (i) for fixed layer thickness, the value of λ_c increases significantly with increasing In composition x in the $In_xGa_{1-x}Sb$ layers, and (ii) the layer thickness required to obtain a given cutoff wavelength decreases with increasing In composition. It is also worth pointing out that, for short-period SL's, the results of tight-binding calculations for E_{gs} are surprisingly similar to the results of the eight-band $\mathbf{k}\cdot\mathbf{p}$ and the EBOM studies.

Concerning the EBOM results, we find that the SL gaps are extremely sensitive to the parameters used. We choose parameters that reproduce the electron, heavy-hole, and light-hole curvatures at the zone center (see Table II). We take the elastic constants and deformation potentials from Mailhiot and Smith.[1] The most important parameter in the model, though, is the E_{sx} matrix element (see Ref. 24 for the EBOM Hamiltonian and associated notation). As Chang[27] has pointed out, if one uses the Lawaetz[29] matrix element one can obtain unphysical bands for large $|\mathbf{k}|$. In addition, the conduction-valence band gap at the X point rises to an extremely large value. As a result, when the bulk materials are layered to form a superlattice, the bonding interaction between orbitals on adjacent layers is quite depressed in energy, and the conduction-band states occur below the conduction band of either constituent material. Similarly, valence-band energies appear above the valence bands of either InAs or $In_xGa_{1-x}Sb$. When the Chang constraint is used; however, the X band gap is much reduced and so the SL energies become reasonable. This choice of contraint also accounts for part of the variation between the EBOM and the $\mathbf{k}\cdot\mathbf{p}$ results. In the $\mathbf{k}\cdot\mathbf{p}$ model, the momentum matrix element is determined by the split-off mass, which we take from experiment. In

TABLE III. Comparison of E_{gs} (meV) from various methods for three InAs/$In_xGa_{1-x}Sb$ SL's (samples are labeled in the notation of Ref. 6).

Sample no.	x value	InAs/$In_xGa_{1-x}Sb$ thickness (Å)	E_{gs} Expt. (Ref. 6)		E_{gs} Calc. ETBM	E_{gs} Calc. k·p	E_{gs} Calc. EBOM
566	0.29	38/24	98±10	97±10	103	124	137
890	0.26	41/25	104±5	111±10	93	118	128
899	0.24	37/25	139±5	152±20	112	136	150

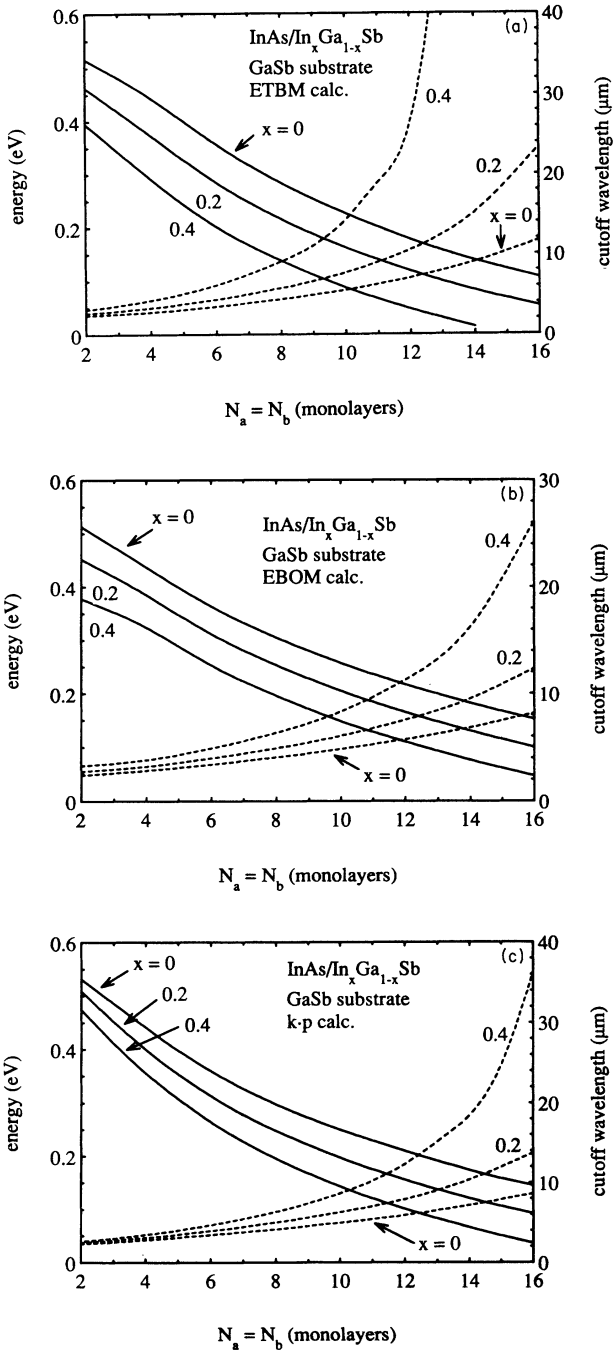

FIG. 1. Calculated results of superlattice band gap E_{gs} (solid line) and cutoff wavelength λ_c (dotted line) as a function of layer thickness ($N_a = N_b$) and composition x in a strained-layer InAs/$In_xGa_{1-x}Sb$ (001) SL grown on a GaSb substrate. (a) ETBM, (b) EBOM, and (c) eight-band **k·p** results.

the EBOM calculation, though, this matrix element is related to E_{sx}. Thus, even though both the EBOM and **k·p** calculations incorporate the same electron, heavy-hole, and light-hole masses, they have different momentum matrix elements, and hence different amounts of *mixing* between the conduction and valence bands away from **k**=**0**. This difference in the *nonparabolicity* causes some of the variation in the calculated results.

To examine this variation between the EBOM and **k·p** models in more detail, we ran both programs without strain and with identical material parameters; we also performed a strain-free ETBM calculation for completeness (see Fig. 2). This time, however, we used the *same* interband matrix element in both the EBOM and **k·p** calculations (we took the EBOM value), thus forcing each to give exactly the same small-|**k**| bulk dispersion for the heavy-hole, light-hole, split-off, and conduction bands. We expected, therefore, that both would give the same energy gaps for any superlattice, especially for longer periods. Indeed, for the InAs/GaSb superlattice, the **k·p** and EBOM calculations yielded very similar results and became almost identical for longer periods. For the InAs/InSb superlattice, however, the EBOM energies were much lower than the **k·p** energies at all thicknesses and the curves approached each other quite slowly as the period increased. Hence, it appears that this narrow-band-gap system magnifies the physical differences between the EBOM and **k·p** models. We also note in passing that the ETBM returned the lowest energies of all at long periods, consistent with the heavier effective masses embedded in this model. We conclude that, because of the extremely small bulk band gaps and the large band offsets, none of the models can reliably calculate the bandgap of InAs/InSb superlattices. It may be possible

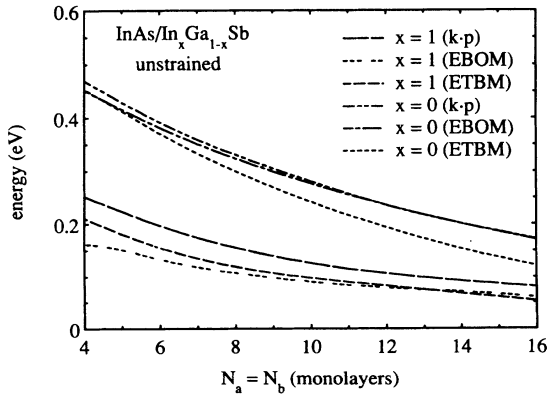

FIG. 2. Comparative study of superlattice band gap E_{gs} as a function of layer thickness ($N_a = N_b$) and composition x in an unstrained InAs/$In_xGa_{1-x}Sb$ (001) SL.

though, to improve the models to allow accurate calculation. For example, more second-nearest neighbors could be added to the ETBM,[30] or more bands to the $\mathbf{k}\cdot\mathbf{p}$ model. In principle, one could also add second-nearest neighbors to the EBOM to improve the accuracy. To maintain the spirit of the model, these parameters should be chosen to preserve the band-edge effective masses.

We now remark upon the somewhat surprising success of the sp^3s^* model in describing very short-period $InAs/In_xGa_{1-x}Sb$ SL's, for small values of x. Since we have made no effort to fit the masses in this tight-binding model, one might expect the computed SL energies to be greatly at variance with experiment. However, since the SL period is quite short, the zone-folding effects become just as important as the effective masses. Thus, since we have fit the Γ, X, and L band gaps accurately in the sp^3s^* model, we obtain reasonable results even though the masses are inaccurate. In particular, the conduction-band mass is too large, and so the ETBM gives band gaps consistently lower than the $\mathbf{k}\cdot\mathbf{p}$ and EBOM models. Since the sp^3s^* model does take into account the difference between the anion and cation states, though, it is difficult to say which model currently gives more accurate results. No doubt the optimal model would employ a tight-binding basis that is fitted to both band gaps and the carrier masses.

IV. SUMMARY AND CONCLUSIONS

In summary, type-II $InAs/In_xGa_{1-x}Sb$ strained-layer superlattices have been explored for an application as long-wavelength infrared detectors using three different theoretical approaches. The effective band gap (E_{gs}) and cutoff wavelength (λ_c) of the material system have been calculated from the modified empirical tight-binding theory, effective-bond-orbital model, and 8×8 $\mathbf{k}\cdot\mathbf{p}$ scheme. For the pure binary, InAs/GaSb, all three model calculations yield very similar results. Differences begin to appear as the band gap of the second layer is reduced via the addition of In. The biggest discrepancies occur for the binary InAs/InSb.

All three model calculations show the same trends and demonstrate that, at least from the standpoint of available band gaps, a wide range of wavelengths could be detected. By appropriate choice of the In composition and layer thicknesses, cutoff wavelengths in the 12–30-μm range are achievable. Design constraints, such as wave-function overlap and dark currents may rule out the use of this system at the longer wavelengths. The calculations indicate that choosing a high In content to obtain a narrow band gap is not necessarily a practical approach to achieve long-wavelength detection, for the results then become very sensitive to the layer thicknesses. Small deviations in the layer thicknesses from the nominal values will produce a band gap that differs substantially from the intended band gap. Longer wavelengths can be achieved by resorting to thicker layers with a small In composition. This approach, however, will result in a smaller detectivity because of the reduced spatial matrix element. It is thus seen that there are a number of conflicting device design constraints. The foregoing calculations are to be regarded as a basis for future work to calculate the absorption coefficient and the dark current of this material system.

ACKNOWLEDGMENTS

The authors thank Professor Y. C. Chang for allowing them to compare the EBOM calculations with the results of his program. This research was performed at Wright Laboratories, Solid State Electronics Directorate (WL/EL), Wright Patterson Air Force Base, OH and was funded in part by the Air Force Office of Scientific Research. The work of D.N.T. was supported by the National Research Council and the work of B.J. was funded by the USAF Contract No. F33615-91C-1765.

APPENDIX

Here we present the details of SL band-structure calculations using a modified ETBM. The SL consists of two different zinc-blende type crystals labeled as (c,a) and (c',a') with a (001) interface. The terms c (c') and a (a') are regarded as the cation and the anion atoms of the A (B) material. Denoting the wave function corresponding to the atoms in the mth sublayer of material A as $|\phi_b(m)\rangle$ (with $b=a$ or c) and that corresponding to the nth sublayer of material B as $|\phi_{b'}(n)\rangle$ (with $b'=a'$ or c') we can write the SL Hamiltonian in the tight-binding (sp^3s^*) basis as

$$
H_{\mathrm{SL}}=\left(\begin{array}{cccccccccc}
1 & 2 & 3 & \cdots & 2^*N_a & 1 & 2 & 3 & \cdots & 2^*N_b \\
\hline
H_a & V_{\mathrm{I}}^A & U_{\mathrm{aa}} & & & & & & hU_{aa'}^* & hV_{\mathrm{II}}^{*C} \\
 & H_c & V_{\mathrm{II}}^A & & & & & & & hU_{cc'}^* \\
 & & H_a & & & & & & & \\
 & & & \ddots & U_{cc} & & & & & \\
 & & & & V_{\mathrm{I}}^A & U_{aa'} & & & & \\
 & & & & H_c & V_{\mathrm{II}}^D & U_{cc'} & & & \\
 & & & & & H_{a'} & V_{\mathrm{I}}^B & U_{a'a'} & & \\
 & & & & & & H_{c'} & V_{\mathrm{II}}^B & & \\
 & & \mathrm{c.c.} & & & & & H_{a'} & \ddots & U_{c'c'} \\
 & & & & & & & & & V_{\mathrm{I}}^B \\
 & & & & & & & & & H_{c'}
\end{array}\right) \tag{A1}
$$

where

$$H_{a(c)}=\langle\phi_{a(c)}(m)|H_{\rm SL}|\phi_{a(c)}(m)\rangle\ ,$$
$$H_{a'(c')}=\langle\phi_{a'(c')}(n)|H_{\rm SL}|\phi_{a'(c')}(n)\rangle\ ,$$
$$V_{\rm I}^{A}=\langle\phi_{a}(m)|H_{\rm SL}|\phi_{c}(m)\rangle\ ,$$
$$V_{\rm II}^{A}=\langle\phi_{c}(m)|H_{\rm SL}|\phi_{a}(m+1)\rangle\ ,$$
$$U_{aa(cc)}=\langle\phi_{a(c)}(m)|H_{\rm SL}|\phi_{a(c)}(m+1)\rangle\ ,$$
$$U_{a'a'(c'c')}=\langle\phi_{a'(c')}(n)|H_{\rm SL}|\phi_{a'(c')}(n+1)\rangle\ ,$$
$$V_{\rm I}^{B}=\langle\phi_{a'}(n)|H_{\rm SL}|\phi_{c'}(n)\rangle\ ,$$
$$V_{\rm II}^{B}=\langle\phi_{c'}(n)|H_{\rm SL}|\phi_{a'}(n+1)\rangle\ ,$$
$$V_{\rm II}^{C}=\langle\phi_{c'}(N_L)|H_{\rm SL}|\phi_{a}(N_L+1)\rangle\ ,$$
$$V_{\rm II}^{D}=\langle\phi_{c}(N_a)|H_{\rm SL}|\phi_{a'}(N_a+1)\rangle\ ,$$
$$U_{aa'}=\langle\phi_{a}(N_a)|H_{\rm SL}|\phi_{a'}(N_a+1)\rangle\ ,$$
$$U_{cc'}=\langle\phi_{c}(N_a)|H_{\rm SL}|\phi_{c'}(N_a+1)\rangle\ ,$$

and

$$h=\exp\left\{\frac{-iN_Lk_za_{\rm SL}}{2}\right\}.$$

Each term in Eq. (A1) is a 5×5 matrix and has the following form

$$H_{a(a')}=\begin{pmatrix} E_{ss}^{a(a')} & 0 & 0 & f_0E_{sx}^{a(a')} & 0 \\ & E_{pp}^{a(a')} & f_0E_{xy}^{a(a')} & 0 & 0 \\ & & E_{p}^{a(a')} & 0 & 0 \\ \text{c.c.} & & & E_{pp}^{a(a')} & 0 \\ & & & & E_{s^*s^*}^{a(a')} \end{pmatrix},$$

$$H_{c(c')}=\begin{pmatrix} E_{ss}^{c(c')} & 0 & 0 & -f_0E_{sx}^{c(c')} & 0 \\ & E_{pp}^{c(c')} & f_0E_{xy}^{c(c')} & 0 & 0 \\ & & E_{pp}^{c(c')} & 0 & 0 \\ \text{c.c.} & & & E_{pp}^{c(c')} & 0 \\ & & & & E_{s^*s^*}^{c(c')} \end{pmatrix},$$

$$V_{\rm I}^{X}=\begin{pmatrix} g_0V_{ss} & g_1V_{s0x} & g_2V_{s0y} & g_3V_{s0z} & 0 \\ -g_1V_{s1x} & g_0V_{xx} & g_3V_{xy} & g_2V_{xz} & -g_1V_{s^*1x} \\ -g_2V_{s1y} & g_3V_{xy} & g_0V_{yy} & g_1V_{yz} & -g_2V_{s^*1y} \\ -g_3V_{s1z} & g_2V_{xz} & g_1V_{yz} & g_0V_{zz} & -g_3V_{s^*1z} \\ 0 & g_1V_{s^*0x} & g_2V_{s^*0y} & g_3V_{s^*0z} & 0 \end{pmatrix},$$

$$V_{\rm II}^{X}=\begin{pmatrix} g_4V_{ss} & -g_5V_{s1x} & -g_6V_{s1y} & -g_7V_{s1z} & 0 \\ g_5V_{s0x} & g_4V_{xx} & g_7V_{xy} & g_6V_{xz} & g_5V_{s^*0x} \\ g_6V_{s0y} & g_7V_{xy} & g_4V_{yy} & g_5V_{yz} & g_6V_{s^*0y} \\ g_7V_{s0z} & g_6V_{xz} & g_5V_{yz} & g_4V_{zz} & g_7V_{s^*0z} \\ 0 & -g_5V_{s^*1x} & -g_6V_{s^*1y} & -g_7V_{s^*1z} & 0 \end{pmatrix},$$

$$U_{aa(a'a')}=\begin{pmatrix} 0 & f_1E_{sx}^{a(a')} & f_2E_{sx}^{a(a')} & 0 & 0 \\ f_1E_{sx}^{a(a')} & 0 & 0 & f_2E_{xy}^{a(a')} & 0 \\ f_2E_{sx}^{a(a')} & 0 & 0 & f_1E_{xy}^{a(a')} & 0 \\ 0 & f_2E_{xy}^{a(a')} & f_1E_{xy}^{a(a')} & 0 & 0 \\ 0 & 0 & 0 & 0 & 0 \end{pmatrix},$$

$$U_{cc}(c'c')=\begin{bmatrix} 0 & -f_1E_{sx}^{c(c')} & -f_2E_{sx}^{c(c')} & 0 & 0 \\ -f_1E_{sx}^{c(c')} & 0 & 0 & f_2E_{xy}^{c(c')} & 0 \\ -f_2E_{sx}^{c(c')} & 0 & 0 & f_1E_{xy}^{c(c')} & 0 \\ 0 & f_2E_{xy}^{c(c')} & f_1E_{xy}^{c(c')} & 0 & 0 \\ 0 & 0 & 0 & 0 & 0 \end{bmatrix},$$

$$U_{aa'}=\begin{bmatrix} 0 & f_1E_{sx}^{\mathrm{av},a} & f_2E_{sx}^{\mathrm{av},a} & 0 & 0 \\ f_1E_{sx}^{\mathrm{av},a} & 0 & 0 & f_2E_{xy}^{\mathrm{av},a} & 0 \\ f_2E_{sx}^{\mathrm{av},a} & 0 & 0 & f_1E_{xy}^{\mathrm{av},a} & 0 \\ 0 & f_2E_{xy}^{\mathrm{av},a} & f_1E_{xy}^{\mathrm{av},a} & 0 & 0 \\ 0 & 0 & 0 & 0 & 0 \end{bmatrix},$$

$$U_{cc'}=\begin{bmatrix} 0 & -f_1E_{sx}^{\mathrm{av},c} & -f_2E_{sx}^{\mathrm{av},c} & 0 & 0 \\ -f_1E_{sx}^{\mathrm{av},c} & 0 & 0 & f_2E_{xy}^{\mathrm{av},c} & 0 \\ -f_2E_{sx}^{\mathrm{av},c} & 0 & 0 & f_1E_{xy}^{\mathrm{av},c} & 0 \\ 0 & f_2E_{xy}^{\mathrm{av},c} & f_1E_{xy}^{\mathrm{av},c} & 0 & 0 \\ 0 & 0 & 0 & 0 & 0 \end{bmatrix}.$$

The explicit forms for g_i $(i=0,1,\ldots,7)$ and f_j $(j=0,1,2)$ are given in Table IV. The strained interatomic matrix elements are derived from the unstrained parameters (cf. Table I) using the following relationships:

$$V_{ss}=\beta V_{ss}^0 ,$$
$$V_{s1x}=\sqrt{3}\beta\cos(\theta_x)V_{s1p}^0 ,$$
$$V_{s1y}=\sqrt{3}\beta\cos(\theta_y)V_{s1p}^0 ,$$
$$V_{s1z}=\sqrt{3}\beta\cos(\theta_z)V_{s1p}^0 ,$$
$$V_{s0x}=\sqrt{3}\beta\cos(\theta_x)V_{s0p}^0 ,$$
$$V_{s0y}=\sqrt{3}\beta\cos(\theta_y)V_{s0p}^0 ,$$
$$V_{s0z}=\sqrt{3}\beta\cos(\theta_z)V_{s0p}^0 ,$$

TABLE IV. Explicit forms for the terms g_i $(i=0,1,\ldots,7)$ and f_j $(j=0,1,2)$ used in Eqs. (A1) and (A2) for calculating the band structure of (001) superlattices. Here a_L is the room-temperature lattice constant of the material A (B).

	g_0	$[\exp i(\mathbf{k}\cdot\tau_1)+\exp i(\mathbf{k}\cdot\tau_2)]/4$
	g_1	$[\exp i(\mathbf{k}\cdot\tau_1)-\exp i(\mathbf{k}\cdot\tau_2)]/4$
	g_2	$-g_1$
	g_3	$-g_0$
	g_4	$[\exp -i(\mathbf{k}\cdot\tau_4)+\exp -i(\mathbf{k}\cdot\tau_3)]/4$
	g_5	$[\exp -i(\mathbf{k}\cdot\tau_4)-\exp -i(\mathbf{k}\cdot\tau_3)]/4$
	g_6	g_5
	g_7	g_4
	f_0	$[\cos\mathbf{k}\cdot(\tau_1-\tau_2)-\cos\mathbf{k}\cdot(\tau_3-\tau_4)]/4$
	f_1	$[\exp i\mathbf{k}\cdot(\tau_2-\tau_3)+\exp i\mathbf{k}\cdot(\tau_1-\tau_4)]/4$
	f_2	$[\exp i\mathbf{k}\cdot(\tau_1-\tau_3)+\exp i\mathbf{k}\cdot(\tau_2-\tau_4)]/4$
where	τ_1/a_L	$(-1,1,1,)/4$
	τ_2/a_L	$(1,-1,1)/4$
	τ_3/a_L	$(1,1,-1)/4$
	τ_4/a_L	$(-1,-1,-1)/4$

$$V_{s^*1y}=\sqrt{3}\beta\cos(\theta_y)V_{s^*1p}^0 ,$$
$$V_{s^*1z}=\sqrt{3}\beta\cos(\theta_z)V_{s^*1p}^0 ,$$
$$V_{s^*0x}=\sqrt{3}\beta\cos(\theta_x)V_{s^*0p}^0 ,$$
$$V_{s^*0y}=\sqrt{3}\beta\cos(\theta_y)V_{s^*0p}^0 ,$$
$$V_{s^*0z}=\sqrt{3}\beta\cos(\theta_z)V_{s^*0p}^0 ,$$
$$V_{xx}=\beta V_{xx}^0+\beta[2\cos^2(\theta_x)-\sin^2(\theta_x)]V_{xy}^0 ,$$
$$V_{yy}=\beta V_{xx}^0+\beta[2\cos^2(\theta_y)-\sin^2(\theta_y)]V_{xy}^0 ,$$
$$V_{zz}=\beta V_{xx}^0+\beta[2\cos^2(\theta_z)-\sin^2(\theta_z)]V_{xy}^0 ,$$
$$V_{xy}=3\beta\cos(\theta_x)\cos(\theta_y)V_{xy}^0 ,$$
$$V_{yz}=3\beta\cos(\theta_y)\cos(\theta_z)V_{xy}^0 ,$$
$$V_{zx}=3\beta\cos(\theta_z)\cos(\theta_x)V_{xy}^0 ,$$
$$E_{sx}^a=\alpha E_{sx}^{0a} ,$$
$$E_{sx}^c=\alpha E_{sx}^{0c} ,$$
$$E_{xy}^a=\alpha E_{xy}^{0a} ,$$
$$E_{xy}^c=\alpha E_{xy}^{0c} ,$$

where

$$\beta=[1+\tfrac{2}{3}(\varepsilon_{xx}+\varepsilon_{yy}+\varepsilon_{zz})+\tfrac{1}{3}(\varepsilon_{xx}^2+\varepsilon_{yy}^2+\varepsilon_{zz}^2)]^{-1} ,$$

$$\alpha=\frac{1}{(1+\varepsilon_{xx})^2} ,$$

and

$$\cos(\theta_\gamma)=\frac{(1+\varepsilon_{\gamma\gamma})}{\sqrt{(1+\varepsilon_{xx})^2+(1+\varepsilon_{yy})^2+(1+\varepsilon_{zz})^2}} .$$

Here $\varepsilon_{xx}(=\varepsilon_{yy})$ and ε_{zz} are the in-plane and vertical strain components, respectively, and $\gamma=x,y,z$.

*Permanent address: Department of Physics, Indiana University of Pennsylvania, Indiana, PA 15705-1087.

[1]C. Mailhiot and D. L. Smith, J. Vac. Sci. Technol. A **7**, 445 (1989).

[2]D. H. Chow, R. H. Miles, J. R. Söderström, and T. C. McGill, Appl. Phys. Lett. **56**, 1418 (1990).

[3]D. H. Chow, R. H. Miles, and A. T. Hunter, J. Vac. Sci. Technol. B **10**, 888 (1992).

[4]J. Shen, S. Y. Ren, and J. D. Dow, Phys. Rev. B **46**, 6938 (1992); Phys. Rev. Lett. **69**, 1089 (1992).

[5]C. H. Grein, P. M. Young, and H. Ehrenreich, Appl. Phys. Lett. **61**, 2905 (1992).

[6]J. P. Omaggio, R. J. Wagner, J. R. Meyer, C. A. Hoffman, M. J. Yang, D. H. Chow, and R. H. Miles, Semicond. Sci. Technol. **8**, S112 (1993), and references therein.

[7]R. H. Miles, J. N. Schulman, D. H. Chow, and T. C. McGill, Semicond. Sci. Technol. **8**, S102 (1993).

[8]C. A. Hoffman, J. R. Meyer, F. J. Bartoli, and W. I. Wang, Phys. Rev. B **48**, 1959 (1993).

[9]J. Katz, Y. Zhang, and W. I. Wang, Appl. Phys. Lett. **62**, 609 (1993).

[10]J. N. Schulman and T. C. McGill, Appl. Phys. Lett. **34**, 603 (1979).

[11]R. M. Biefeld, C. R. Hills, and S. R. Lee, J. Cryst. Growth **91**, 515 (1988).

[12]S. R. Kurtz, G. C. Osbourn, R. M. Biefeld, and S. R. Lee, Appl. Phys. Lett. **53**, 216 (1988).

[13]S. R. Kurtz, R. M. Biefeld, L. R. Dawson, I. J. Fritz, and T. E. Zipperian, Appl. Phys. Lett. **53**, 1961 (1988).

[14]S. R. Kurtz and R. M. Biefeld, Phys. Rev. B **44**, 1143 (1991).

[15]G. A. Sai-Halasz, R. Tsu, and L. Esaki, Appl. Phys. Lett. **30**, 651 (1977).

[16]P. Vögl, H. P. Hjalmarson, and J. D. Dow, J. Phys. Chem. Solids **44**, 365 (1983).

[17]K. E. Newman and J. D. Dow, Phys. Rev. B **30**, 1929 (1984).

[18]E. Yamaguchi, J. Phys. Soc. Jpn. **57**, 2461 (1988).

[19]W. A. Harrison, *Electronic Structure and the Properties of Solids* (Freeman, San Francisco, 1980).

[20]Y. Wu, S. Fujita, and S. Fujita, J. Appl. Phys. **67**, 908 (1990).

[21]E. O. Kane, *Physics of III-V Compounds* (Academic, New York, 1966), Vol. 1, Chap. 3, pp. 75–100.

[22]T. B. Bahder, Phys. Rev. B **41**, 11 992 (1990); **46**, 9913(E) (1992).

[23]G. E. Pikus and G. L. Bir. Fiz. Tverd. Tela (Leningrad) **1**, 1642 (1959) [Sov. Phys. Solid State **1**, 1502 (1959)].

[24]F. H. Pollak and M. Cardona, Phys. Rev. **172**, 816 (1967).

[25]The finite-difference technique is quite well known. See, for example, C. F. Gerald, *Applied Numerical Analysis* (Addison-Wesley, Reading, MA, 1980).

[26]M. Altarelli, in *Heterojunctions and Semiconductor Superlattices,* Proceedings of the Les Houches Winter School, France, 1985, edited by G. Allan, G. Bastard, N. Boccara, M. Lannoo, and M. Voos (Springer-Verlag, Berlin, 1986).

[27]Y. C. Chang, Phys. Rev. B **37**, 8215 (1988).

[28]J. N. Schulman and T. C. McGill, Phys. Rev. Lett. **39**, 1680 (1977); Appl. Phys. Lett. **34**, 663 (1979).

[29]P. Lawaetz, Phys. Rev. B **4**, 3460 (1971).

[30]D. N. Talwar and C. S. Ting, Phys. Rev. B **25**, 2660 (1982).